Absolute generalized-oscillator-strength measurement of preionization-edge electronic excitations in the valence and $2p$ shells of argon

X. W. Fan and K. T. Leung*
Department of Chemistry, University of Waterloo, Waterloo, Ontario, Canada N2L 3G1
(Received 2 August 2000; published 3 November 2000)

Absolute generalized oscillator strengths (GOS's) of the $3p^6 \rightarrow 3p^5(4s,4s')$, $3p^6 \rightarrow 3p^5(4p,4p')$, and $3p^6 \rightarrow 3p^5(5s,5s',3d,3d')$ valence-shell electronic transitions as well as the $2p_{3/2} \rightarrow 4s$ inner-shell transition in Ar have been determined as functions of energy loss and momentum transfer (K) at an impact energy of 2.5 keV. Generally good agreement can be found between the present GOS measurement for the $3p^6 \rightarrow 3p^5(4s,4s')$ transitions (at 11.8 eV) and the previous experimental profiles for $K<1$ a.u. Calculations based on the first Born approximation appear to be in reasonable agreement with the GOS data only in shape and also for $K<1$ a.u., while the Yukawa frozen-core calculations based on the Glauber approximation appear to converge to the present data even for $K>1$ a.u. The experimental and theoretical results all give consistent values for the K positions of the observed minimum and maximum in the GOS profile of the $3p^6 \rightarrow 3p^5(4s,4s')$ transitions. The GOS profile for the $3p^6 \rightarrow 3p^5(4p,4p')$ transitions (at 13.4 eV) in Ar has been determined and found to have a shape characteristic of nondipole excitation with a maximum at $K^2 \sim 0.7$ a.u. Like the $3p^6 \rightarrow 3p^5(4s,4s')$ transitions, the GOS profile for the $3p^6 \rightarrow 3p^5(5s,5s',3d,3d')$ transitions (at 14.2 eV) has the characteristic dipole-dominated shape with a strong maximum at $K=0$ but a notably larger width and without any discernible extrema. Finally, the GOS profile for the $2p_{3/2} \rightarrow 4s$ inner-shell transition (at 244.4 eV) is dominated by a strong maximum at $K=0$, characteristic of generally dipole-allowed excitations, but with a broad and rather complex shape. The present work illustrates the analytical value of GOS profiles for probing the intricate nature of the valence- and inner-shell electronic excitations.

PACS number(s): 34.50.Fa, 34.80.Dp

I. INTRODUCTION

Absolute cross section or generalized-oscillator-strength (GOS) information for both valence- and inner-shell excitation of atoms and molecules is of great importance in such diverse fields as radiation physics, plasma research, atmospheric science, astrophysics, and laser development. According to the Bethe theory [1], the cross section for a sufficiently fast electron collision can be factorized into a scattering factor involving the kinematics of the electron before and after the collision, and the transition probability or GOS of the electron-impact excitation of the target. GOS measurements as a function of momentum transfer (K), i.e., away from the dipole limit, offer unique information about the nature of the electronic transitions and of the electron-scattering process itself. The GOS profile of an individual transition provides a detailed ''mapping'' of the overlap function between the initial-state and final-state wave functions in momentum space, which can be used for spectral assignments, better understanding of the nature of underlying interactions, and detailed evaluation of the quality of wave functions of the initial state and final state, as well as for the development of new quantum computational methods [2,3]. Pioneered by Lassettre and co-workers, angle-resolved electron-energy-loss spectroscopy (EELS) has been used quite extensively to determine precise dipole oscillator strength (DOS) by extrapolating the GOS profile to the optical limit ($K=0$) [4]. One practical advantage of angle-resolved EELS over photoabsorption spectroscopy is the prospect of obtaining precise absolute cross-section data over a wide energy range without performing an ''absolute'' experiment [5]. Angle-resolved EELS therefore offers a powerful, absolute method for comprehensive investigation of all the possible electronic excitations involving both dipole-allowed and optically inaccessible nondipole states in the valence and inner shells [6–9].

Angle-resolved EELS spectra for noble atoms up to 450-eV energy loss and a scattering angle of 12° were first obtained at 3–4-keV impact energy by Afrosimov *et al.* [10]. The valence-shell electronic structure of Ar has been studied extensively by a variety of techniques, including photoabsorption [11–13], small-angle EELS [14] and angle-resolved EELS [15–18]. In particular, the $3p^6 \rightarrow 3p^5(4s,4s')$ low-lying electronic transitions in Ar have attracted a lot of theoretical and experimental attention not only because of their practical interest to plasma research and laser development but also due to the existence of minimum and maximum in the GOS profile. It has been suggested that the positions of these GOS extrema are related to the nodal properties of the radial parts of the orbital wave functions of the initial and final states. The first comprehensive experimental study of the GOS extrema for the $np(n+1)s$ transitions of noble atoms, including the aforementioned $3p^6 \rightarrow 3p^5(4s,4s')$ transitions in Ar, covering a wide momentum-transfer range (up to 3 a.u.) was made by Wong *et al.* at 25-keV impact energy [16]. The relative GOS profile determined by Wong *et al.* [16] showed that the positions of these extrema are in excellent agreement with an earlier reported Hartree-Fock calculation [19]. Using a high-resolution EELS spectrometer (with

*Electronic address: tong@uwaterloo.ca

25–40-meV energy resolution), Li *et al.* were able to determine separate absolute GOS profiles for the $3p^6 \rightarrow 3p^5 4s$ and $3p^6 \rightarrow 3p^5 4s'$ transitions [17]. However, due to the relatively low impact energies (400 and 500 eV) employed, the momentum-transfer range was limited to less than 1 a.u., which did not permit observation of the GOS extrema [17]. Later, Bielschowsky *et al.* reported absolute GOS values of the $3p^6 \rightarrow 3p^5(4s,4s')$ electronic transitions for momentum transfer up to 2.23 a.u. at 1-keV impact energy [18].

Using the first Born approximation and numerical Hartree-Fock wave functions, Bonham predicted the existence of these GOS extrema for the $3p^6 \rightarrow 3p^5(4s,4s')$ transitions in Ar [19]. This theoretical work was later extended by Shimamura, who used hydrogenlike wave functions to obtain the analytical forms of the GOS [20]. In the meantime, Ganas and Green calculated GOS's for the single-particle excitations of Ne, Ar, and Xe, utilizing the analytic atomic independent-particle model of Green, Sellin, and Zachor as a basis [21]. Using the Glauber approximation, Bielschowsky *et al.* calculated the GOS profile by taking into consideration the interaction between the incident electron first with only the atomic electron that participates directly in the excitation process and one nuclear charge [inert frozen-core (IFC) calculation], and additionally with the atomic electrons not directly involved in the excitation process and the $(N-1)$ nuclear charges via the Yukawa potential [Yukawa frozen-core (YFC) calculation] [18]. All these calculations give generally good agreement with the experiments reported to date for the DOS, positions of the GOS extrema, and the GOS profile for $K<1$ a.u.

Among the various experimental and theoretical GOS values reported to date for the well-known lowest-lying electronic transitions in Ar, there remains notable unresolved discrepancy among the results, especially in the higher momentum-transfer region ($K>1$ a.u.). Furthermore, almost all of the existing studies on Ar have focused on these particular $3p^6 \rightarrow 3p^5(4s,4s')$ electronic transitions. No absolute GOS measurement has been reported for the other (next low-lying) preionization-edge electronic transitions in Ar, including, e.g., the dipole-forbidden $3p^6 \rightarrow 3p^5(4p,4p')$ and dipole-allowed $3p^6 \rightarrow 3p^5(5s,5s')$ and $3p^6 \rightarrow 3p^5(3d,3d')$ transitions in the valence shell, as well as the $2p \rightarrow 4s$ transition in the inner shell. In addition, the GOS measurements published to date for the $3p^6 \rightarrow 3p^5(4s,4s')$ transitions were made absolute by normalizing to the available absolute elastic cross sections [17,18]. It would therefore be of great interest to have an independently normalized data set to provide a separate assessment of the absolute accuracy of the available data.

In the past several years, angle-dependent EELS has been used in our laboratory to study the electronic structure of the valence and inner shells of a large number of polyatomic molecules, particularly chlorofluorocarbons and chlorofluorohydrocarbons [22]. A recent review of our work and this area has been given by Leung [23]. Most recently, we have extended our study to include the autoionizing resonances in He [24] and Ar [25], and determined the momentum-transfer dependence of the Fano parameters. The present work provides a measurement of the absolute GOS profiles for the aforementioned low-lying preionization-edge transitions in the valence and $2p$ shells of Ar, which may collectively shed further insights into the electron-impact electronic excitation of noble atoms.

II. THEORETICAL BACKGROUND

A typical inelastic electron-scattering process involves the promotion of an atomic or molecular target from its electronic ground state (M) to an excited state (M^*) by transfers of energy and momentum from an incident electron,

$$e^-(E_0,\mathbf{k}_0)+M \rightarrow e^-(E_0-E,\mathbf{k})+M^*, \tag{1}$$

where E_0 (or E_0-E) and $\mathbf{k}_0$ (or $\mathbf{k}$) are the kinetic energy and momentum of the incident (or scattered) electron, respectively. The magnitude of the momentum transfer $\mathbf{K}(=\mathbf{k}_0-\mathbf{k})$ is related to the scattering angle θ by $K^2=k_0^2+k^2-2k_0k\cos\theta$. The intensity of the scattered electron with an energy loss E at a scattering angle θ is proportional to the differential cross section $d^2\sigma/d\Omega dE$. For high-energy electron collisions, the influence of the incident electron upon the target can be regarded as a sudden and impulsive encounter. In the first Born approximation, the differential GOS, $df(K,E)/dE$, is related to the differential cross section by the Bethe-Born formula (in Rydberg atomic units) [2,3]:

$$\frac{df(K,E)}{dE}=\frac{k_0}{k}K^2\frac{E}{4}\frac{d^2\sigma}{d\Omega dE}, \tag{2}$$

where $d\Omega$ corresponds to the detection solid angle. The GOS, $f(K,E)$, is defined as

$$f(K,E)=\frac{E}{K^2}\left|\left\langle \Psi_n\left|\sum_{j=1}^{N}\exp(i\mathbf{K}\cdot\mathbf{r}_j)\right|\Psi_0\right\rangle\right|^2, \tag{3}$$

where Ψ_0 and Ψ_n are the (N-electron) electronic wave functions of the initial and final states, respectively, and $\mathbf{r}_j$ is the position of the jth electron with respect to the center of mass of the target. For angle-dependent studies that involve finite momentum transfers, Lassettre and coworkers [26] have pointed out that the GOS for a bound-state excitation can be expanded as an even power series of K (the so-called Lassettre series),

$$f(K,E)=\frac{1}{(1+x)^6}\sum_{n=0}^{m}f_n\left(\frac{x}{1+x}\right)^n, \tag{4}$$

where $x=K^2/(\sqrt{2I}+\sqrt{2|I-W|})^2$, I is the ionization potential, and W is the excitation energy of the discrete transition. The integer m $(=2-5)$ is chosen according to the available data and the accessible experimental range of momentum transfer. In the limit when K approaches zero, the GOS approaches the DOS, f_0. The original Lassettre series has been used quite successfully for the quantitative estimate of the DOS values by extrapolating the measured GOS data to zero momentum transfer. The other parameters f_n in the Lassettre series are related to linear combinations of the respective multiple matrix elements and can be used to characterize the

nature of the underlying excitation. Finally, the GOS at any K value can be made absolute independently by using the Bethe sum rule [3]:

$$\int \frac{df(K,E)}{dE} dE = N, \tag{5}$$

where N is the total number of electrons in the target.

III. EXPERIMENTAL DETAILS

The experimental technique and the apparatus used for the present angle-resolved EELS measurement have been described in detail elsewhere [9]. Briefly, a collimated electron beam was accelerated to 2.5-keV impact energy and crossed with a gas jet expanded from a nozzle (0.5-mm diameter) positioned at 1 cm above the collision center. Electrons scattered with an energy loss E at a scattering angle θ (from the forward direction) were analyzed using a hemispherical energy analyzer equipped with a seven-element input lens. The angular divergence of the incident electron beam has been improved substantially by placing a smaller defining aperture of 1.5 mm in diameter at the exit of the collimator. The static gas cell has also been upgraded with a 25-mm-diam cylindrical cage to achieve a more uniform, higher gas density at the collision center without increasing the working pressure. These minor modifications, along with the use of a higher gain electron multiplier, provided marked improvements to the signal-to-background performance and overall collection efficiency of our spectrometer. For the present work, our spectrometer was operated with an optimal energy resolution of 0.8-eV full width at half maximum (FWHM) and an improved angular resolution of 0.2° half-angle.

Angle-resolved EELS spectra of the sample gas introduced to the center of the collision cell (sample spectra) were collected at a series of θ angles (corresponding to different momentum transfers) sequentially in repetitive scans. After each measurement of the sample spectra, an identical set of EELS spectra of the sample gas introduced outside the collision cell at the same pressure $[(1-2)\times 10^{-5}\,\mathrm{Torr}]$ were recorded in the same energy loss and angular ranges (ambience spectra). Contributions from the ambient gas were removed by subtracting the corresponding ambience spectra from the sample spectra after appropriate normalization. This correction of the ambience contribution is very important to precise GOS measurement especially for dipole-forbidden transitions near the forward-scattering angle and for inner-shell and other electronic transitions with low cross sections. For targets and/or transitions with inherently low cross sections, it is often necessary to signal-average a set of sample or ambience spectra over a long period of time, after which the beam condition, the gain of the detector, and other experimental conditions may not be the same as that for the subsequent set of measurements. This difficulty can be resolved by limiting the data acquisition, in a separate run used just for intensity calibration, to just one sample and one ambience spectrum (at a preselected angle). Using these two spectra collected over a much shorter period of time, the intensities of the sample spectra and ambience spectra in the large data sets can then be appropriately adjusted, and the contributions due to the ambient gas can be removed correctly from the sample spectra with confidence.

After the EELS spectra were relatively normalized to one another, the intensity (corresponding to the relative differential cross section) could be converted to relative GOS using the Bethe-Born formula [Eq. (2)] and put on an absolute scale using the Bethe sum rule [Eq. (5)]. In the Bethe sum-rule normalization procedure, the intensity of the relative GOS obtained at a particular momentum transfer is first numerically integrated over a sampling energy loss range of 160 eV. The remaining intensity of the valence shell above 160 eV is estimated by integration of a fitted function $B(E)=A/E^{\nu}$ from 160 eV to infinity, where the empirical constants A and ν are obtained by curve fitting $B(E)$ to the experimental data between 70 and 160 eV [9]. The sum of these two integrated intensities is then normalized to the number of valence-shell electrons (eight for Ar), plus an appropriate correction of the contribution due to Pauli-excluded transitions from the inner shells (0.47 for Ar) [27,28]. Although the momentum transfer is not constant over the entire energy-loss range in a typical EELS spectrum (usually collected at a fixed scattering angle), the variation of the momentum transfer with respect to the energy loss can be ignored if a sufficiently high impact energy is used. Within the present experimental angular range (1.5°–9.5°), the corresponding momentum transfer is found to be effectively constant over the entire (300-eV) energy-loss range used in the present work at 2.5-keV impact energy. As long as the Born approximation is valid, EELS spectra collected at different scattering angles (or momentum transfers) can in principle be normalized individually by using the Bethe sum rule. In practice, however, the Bethe-sum-rule normalization procedure becomes more difficult to apply at higher momentum transfer due to the slow falloff of the continuum at higher energy loss and to the much smaller cross section, making it difficult to reduce the absolute error in the high energy-loss region. For this reason, we generally applied the Bethe-sum-rule normalization only to the EELS spectra collected near the optical limit in the present work.

The angular scale has been calibrated by comparing the measured GOS's of the preionization-edge $1s^2 \rightarrow 1s2s$ and $1s^2 \rightarrow 1s2p$ bound transitions of He with reliable *ab initio* calculations of Kim and Inokuti [29]. A series of EELS spectra were taken at different scattering angles sequentially in repetitive scans in order to obtain self-normalized relative cross sections for these transitions. Two Gaussian profiles were used to estimate the intensities of the quadrupole-allowed $1s^2 \rightarrow 1s2s$ (at 20.6 eV) and the dipole-allowed $1s^2 \rightarrow 1s2p$ transitions (at 21.2 eV). The GOS values have been obtained from the areas of the fitted Gaussian peaks and were made absolute by applying the Bethe sum-rule normalization to the EELS spectrum measured at 1.5°. The excellent agreement between the experiment and calculation shown in Fig. 1 reaffirms the reliability of our measurements over the entire experimental angular range of 1.5°–9.5°. It should be noted that no geometrical correction was found to be necessary for the ''short'' experimental angular range and the high-impact energy employed in the present work.

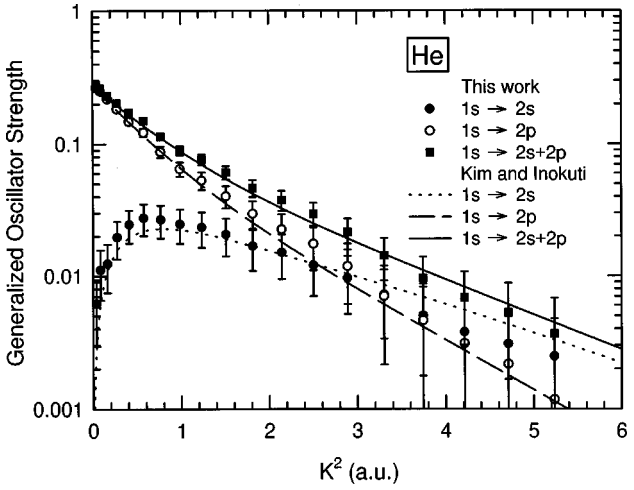

FIG. 1. Absolute generalized oscillator strength profiles of the $1s^2 \rightarrow 1s2s$ (20.6 eV) and $1s^2 \rightarrow 1s2p$ (21.2 eV) transitions in He. The experimental generalized oscillator strengths have been made absolute by applying the Bethe-sum-rule normalization procedure to the EELS spectrum measured at 1.5° and are compared with the *ab initio* calculations by Kim and Inokuti [29].

IV. RESULTS AND DISCUSSION

A. Valence-shell electronic structure of Ar

Within the framework of the first Born scattering theory, a plot of the GOS as a function of energy loss and the logarithm to the base e of the square of the momentum transfer defines the so-called Bethe surface. The Bethe surface contains all the information about the inelastic electron-scattering process with an atom or molecule, and is particularly useful for analyzing such quantities as stopping power, total inelastic scattering cross section, the Compton profile, and polarizability [3]. Figure 2 shows the EELS spectra in the valence-shell region of Ar collected in steps of 0.5° from 1.5° to 9.5° in the form of a Bethe surface plot. These EELS spectra have been obtained relatively normalized to one another and made absolute by applying the Bethe-sum-rule normalization to the spectrum at 1.5°. In the impact-scattering domain of large momentum transfer and energy loss (which corresponds to the kinematical region for ''close'' collisions), a broad ridge is seen to disperse to a higher energy loss with increasing momentum transfer. This ridge is the result of momentum conservation in the inelastic electron-atom collision and becomes the well-known Bethe ridge in the Born approximation. The energy dispersion of this ridge with respect to K is related to manifestation of different Fourier transform components of the overlap density between the initial-state and final-state wave functions [3]. On the other hand, the dipole-scattering domain of small momentum transfer and energy loss exhibits sharp ''optical'' features of the valence shell. This domain is related to ''distant'' collisions, which are mainly governed by dipole interaction. In addition to the prominent preionization-edge single-excitation features, we also observe a number of autoionizing resonances in the inner-valence-shell region (near 27 eV). The momentum-transfer dependence of these so-called ''window'' resonances of Ar will be the subject of a follow-up paper [25].

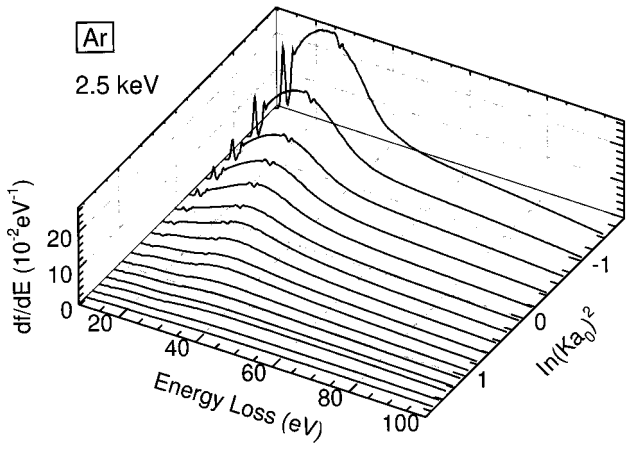

FIG. 2. Bethe surface of the valence shell of Ar determined at 2.5-keV impact energy. Absolute angle-resolved electron-energy-loss spectra were collected in steps of 0.5° from 1.5° to 9.5° repetitively in sequence scans and have been made absolute by applying the Bethe-sum-rule normalization procedure to the 1.5° spectrum.

B. GOS profiles of the lowest-lying preionization-edge electronic transitions of Ar

Figure 3 shows selected valence-shell EELS spectra of Ar collected in the energy-loss range of 10–20 eV at 1.5°, 3.0°, 5.0°, and 8.0°, which correspond to momentum transfers of 0.36, 0.71, 1.18, and 1.89 a.u., respectively. These spectra have been Bethe-Born-corrected and normalized as discussed above. In particular, the preionization-edge features (features 1–4) have been fitted with four Gaussian peaks at 11.8, 13.4, 14.2, and 15.2 eV. The fifth peak located at 15.8 eV is used to better simulate the contribution from the on-set of the $(3p)^{-1}$ ionization edge and the corresponding near-edge structure. The widths of the Gaussian line shapes are estimated from the photoabsorption spectra reported in the literature [11–13], after taking our instrumental energy resolution into account. The assignments for these prominent excitation features of Ar have been given in detail elsewhere [14,15,18]. In particular, feature 1 at 11.8 eV mainly consists of an admixture of dipole-allowed electronic transitions from the $3p^6$ ground state to the $3p^5 4s$ and $3p^5 4s'$ excited states [i.e., the lowest-lying $3p^6 \rightarrow 3p^5(4s,4s')$ transitions]. Feature 2 at 13.4 eV corresponds to dipole-forbidden transitions to the $3p^5 4p$ and $3p^5 4p'$ states. Feature 3 at 14.2 eV and feature 4 at 15.2 eV can be attributed to admixtures of dipole-allowed transitions to the $3p^5 5s$, $3p^5 5s'$, $3p^5 3d$, and $3p^5 3d'$ states and to the $3p^5 6s$, $3p^5 6s'$, $3p^5 4d$, and $3p^5 4d'$ states, respectively.

Evidently, there is a general reduction in the overall spectral intensity of the entire spectrum with increasing momentum transfer. The observed changes in the spectral intensities of the respective features as a function of momentum transfer are consistent with the above assignments. In particular, the intensities of features 1, 3, and 4 are seen to decrease rapidly with increasing momentum transfer, which is characteristic of the dipole-allowed nature of the underlying transitions. On

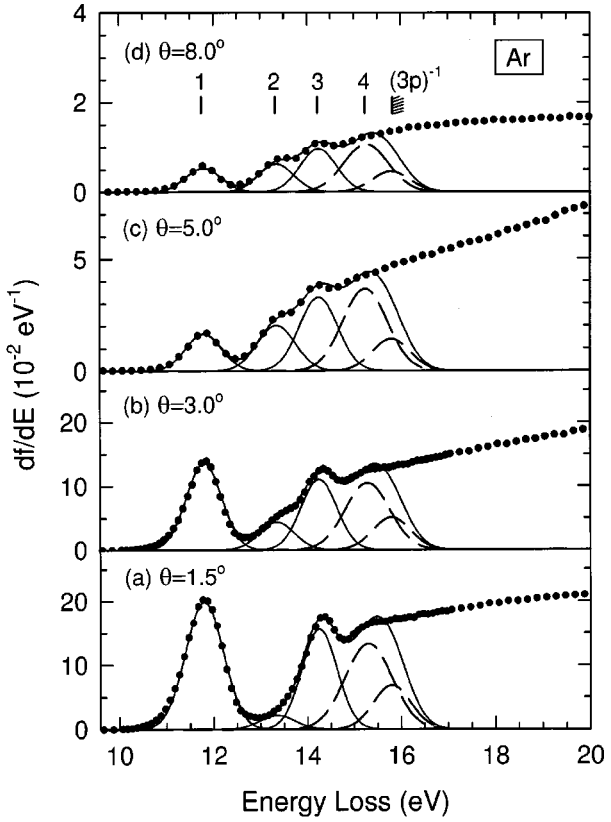

FIG. 3. Absolute angle-resolved electron-energy-loss spectra for the valence shell of Ar measured at (a) 1.5°, (b) 3.0°, (c) 5.0°, and (d) 8.0°. Five Gaussian profiles are used to estimate the intensities of the structures at 11.8 eV (feature 1), 13.4 eV (feature 2), 14.2 eV (feature 3), 15.2 eV (feature 4), and 15.8 eV (ionization edge) in a curve-fitting procedure. Only the first three lowest-lying features are used to estimate the respective generalized oscillator strength profiles.

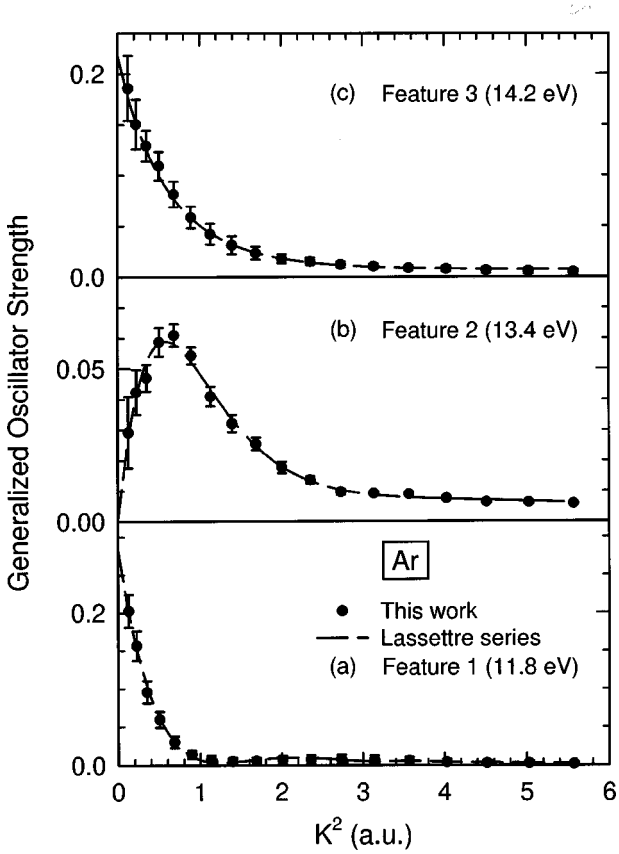

FIG. 4. Absolute generalized oscillator strength as a function of momentum transfer (K) squared for the features at (a) 11.8 eV, (b) 13.4 eV, and (c) 14.2 eV in Ar. The dashed lines correspond to semiempirical fits using the Lassettre series.

the other hand, the peak at 13.4 eV (feature 2), though weak when compared to the neighboring peaks at 11.8 eV (feature 1) and 14.2 eV (feature 3) in the 1.5° spectrum [Fig. 3(a)], becomes more intense in the spectra at larger angles [Figs. 3(a)–3(c)]. The changes in the relative intensity of feature 2 with momentum transfer therefore reflect the nondipole nature of the quadrupole excitation.

The nature of the transitions assigned to these low-lying preionization-edge features can be more quantitatively characterized by examining their respective GOS profiles. The GOS's of these features can be obtained by computing the areas under the corresponding Gaussian peaks in the absolute EELS spectra collected at different scattering angles (as, e.g., in Fig. 3). The resulting experimental GOS profiles can also be fitted semiempirically using the Lassettre series and be used to extrapolate to $K=0$ to obtain the DOS's.

Figure 4 compares the GOS profiles of the preionization-edge excitation features of Ar at 11.8 eV (feature 1), 13.4 eV (feature 2), and 14.2 eV (feature 3). The GOS profile of feature 1, corresponding to the $3p^6 \rightarrow 3p^5(4s,4s')$ transitions, has been investigated quite extensively. As demonstrated by the high-resolution EELS study of Li *et al.* [17], the GOS profiles for the individual $3p^6 \rightarrow 3p^5 4s$ and $3p^6 \rightarrow 3p^5 4s'$ transitions are not simply proportional to each other but have slightly different shapes, both of which are characteristic of dipole-allowed interactions. The calculated and experimental GOS profiles for feature 1 (representing the contribution from both transitions) reported by other workers are compared with the present work in a log-log plot in Fig. 5. A minimum at $K^2=1.35$ a.u. followed by a maximum at $K^2=2.79$ a.u. in our experimental GOS profile is clearly discernible in Fig. 4(a). As shown more clearly in Fig. 5, there is generally good accord on the positions of the GOS extrema between our data and other calculations and experiments. In particular, the positions of the GOS minimum and maximum are in excellent agreement with those ($K^2=1.44$ and 2.86 a.u.) predicted by the calculation by Bonham [19] and with those ($K^2=1.25$ and 2.96 a.u.) obtained experimentally by Wong *et al.* [16] and Bielschowsky *et al.* [18]. Furthermore, although good agreement can be found in the general GOS curve between the present result and the experimental data of Bielschowsky *et al.* for $K<1$ a.u. [18], there is a notable discrepancy in the higher momentum-transfer region. The relative GOS profile measured by Wong *et al.*, when normalized to our data arbitrarily at $K^2=0.69$ a.u., shows a greater discrepancy for $K>1$ a.u. In the case of Wong *et al.*, their primary goal was to identify the positions of GOS extrema for this lowest-lying electronic transition in Ar, and the observed discrepancy in the GOS

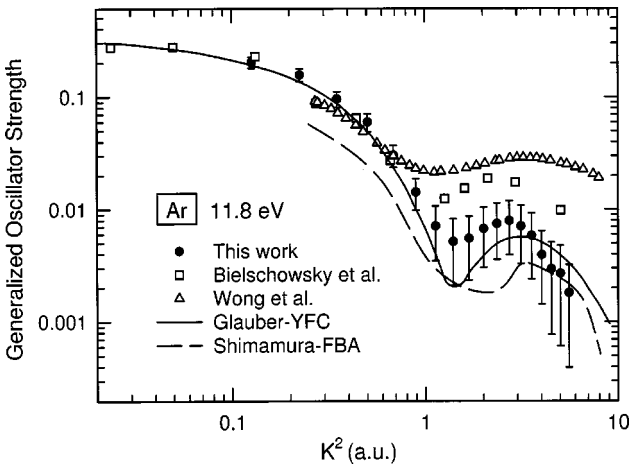

FIG. 5. Absolute generalized oscillator strength as a function of momentum transfer (K) squared for the $3p^6 \rightarrow 3p^5(4s,4s')$ transitions (at 11.8 eV) in Ar. The present data are compared with the experimental results of Bielschowsky *et al.* [18] and Wong *et al.* [16] and with the calculations based on the Glauber-Yukawa frozen-core (YFC) approximation by Bielschowsky *et al.* [18] and on the first Born approximation (FBA) by Shimamura [20]. The relative profile obtained by Wong *et al.* [16] is arbitrarily normalized to the present data at $K^2 = 0.69$ a.u. to facilitate the present comparison.

profile may be due to incomplete removal of the background. Similarly, the calculation by Shimamura [20] can only reproduce the general shape of the experimental data for $K < 1$ a.u. The considerably better agreement between our data and the Glauber-YFC calculation by Bielschowsky *et al.*, which took into account the interaction of the incident electron with the $(N-1)$ nuclear charges and with the atomic electrons that do not participate directly in the excitation process [18], confirms the importance of inclusion of electron correlation effects in the GOS calculations. Finally, the DOS value (0.28) for the $3p^6 \rightarrow 3p^5(4s,4s')$ transitions estimated by the extrapolation of the corresponding GOS profile to $K=0$ using the Lassettre fit is found to be in good accord with the theoretical values (0.290–0.359) [18,30–32] and other experimental results (0.270–0.331) [14,18,33–35].

Figure 4(b) depicts the first experimental measurement of the GOS profile of the $3p^6 \rightarrow 3p^5(4p,4p')$ transitions, which correspond to the lowest-lying dipole-forbidden, quadrupole-allowed preionization-edge electronic excitation in Ar. The presence of a relative maximum at nonzero momentum transfer is a common characteristic of nondipole transitions observed to date [23]. To the best of our knowledge, only a very limited amount of data is available for these types of nondipole transitions in atoms and molecules [23]. The present GOS profile appears to have one of the lowest positions for the GOS maximum (at $K^2 = 0.7$ a.u.), in comparison with the other nondipole valence-shell transitions, including the Lyman-Birge-Hopfield band ($a\ ^1\Pi_g \leftarrow X\ ^1\Sigma_g^+$) in N_2 at 9.3 eV with a GOS maximum at $K^2 = 0.8$ a.u., and the lowest-lying $n(\mathrm{Cl}\ 3p) \rightarrow \sigma^*(\mathrm{C\text{-}Cl})$ transitions in various chlorofluorocarbons and chlorofluorohydrocarbons with GOS maxima at $K^2 = 0.8$–1.1 a.u. [23]. The GOS profile of the present $3p \rightarrow 4p$ transition in Ar is also quite different in shape from the considerably broader profile of the nondipole $1s \rightarrow 2s$ transition in He (Fig. 1), despite the similarity in the locations of their respective GOS maxima (both at $K^2 = 0.7$ a.u.). The Lassettre series can again be used as a means to semiempirically characterize the momentum-transfer dependence of the GOS profiles for these transitions. For example, the f_1 coefficient in the Lassettre series expansion [Eq. (4)] is related to the quadrupole interaction, while the other higher-order coefficients give measures of the other multipole contributions [36]. If the DOS (f_0) is vanishingly small, a quadrupole transition can be characterized by a positive f_1 term, in contrast to a dipole transition with a negative f_1 term. The values for the f_n coefficients obtained in our Lassettre series expansion for the present $3p^6 \rightarrow 3p^5(4p,4p')$ transitions are consistent with the underlying quadrupole interaction [37]. Given the computational attraction of a noble atom, the present GOS profile of Ar offers an interesting benchmark for theoretical modeling of ''prototypical'' $p \rightarrow p$ transitions in atomic systems.

The GOS profile corresponding to the admixture of $3p^6 \rightarrow 3p^5(5s,5s',3d,3d')$ transitions in Ar is also shown in Fig. 4(c). Evidently, the sharp maximum at $K=0$ and the general shape of this GOS profile are characteristic of predominantly dipole-allowed transitions. The DOS estimated by extrapolation of the GOS profile to zero momentum transfer using the Lassettre fit is found to be 0.22, which is in good accord with the theoretical (0.223–0.259) [31,32] and other experimental results (0.201–0.241) [14,33,35]. It is of interest to compare the overall shapes of the two GOS profiles for the low-lying dipole-allowed transitions in Ar observed thus far. In particular, the GOS profile of the $3p^6 \rightarrow 3p^5(5s,5s',3d,3d')$ transitions [feature 3 and Fig. 4(c)] in Ar is found to be significantly broader than that of the $3p^6 \rightarrow 3p^5(4s,4s')$ transitions [feature 1 and Fig. 4(a)]. The apparent increase in the higher momentum-transfer components (or correspondingly more gradual fall-off in the lower momentum-transfer components) of the GOS profile for the $3p^6 \rightarrow 3p^5(5s,5s',3d,3d')$ transitions is clearly related to the differences in the sets of contributing transitions involving different final-state wave functions. Unlike the $3p^6 \rightarrow 3p^5(4s,4s')$ transitions, there is also no discernible extrema in the GOS profile in the case of the $3p^6 \rightarrow 3p^5(5s,5s',3d,3d')$ transitions. According to the high-resolution, small-angle EELS study of Chan *et al.* [14], the sums of the DOS values for the $3p^6 \rightarrow 3p^5 5s$ (at 14.090 eV) and $3p^6 \rightarrow 3p^5 5s'$ transitions (at 14.255 eV) and for the $3p^6 \rightarrow 3p^5 3d$ (at 14.153 eV) and $3p^6 \rightarrow 3p^5 3d'$ transitions (at 14.304 eV) are 0.0390 and 0.197, respectively. Since the DOS for the $3p^6 \rightarrow 3p^5(3d,3d')$ transitions is approximately five times that of the $3p^6 \rightarrow 3p^5(5s,5s')$ transitions, the GOS profile for the $3p^6 \rightarrow 3p^5(5s,5s',3d,3d')$ transitions should therefore be dominated by the constituent GOS profile for the $3p^6 \rightarrow 3p^5(3d,3d')$ transitions. The differences found in the shape of the GOS profile for feature 1 [Fig. 4(a)] and feature 3 [Fig. 4(c)] directly reflect the differences in the corresponding predominant excited-state wave functions

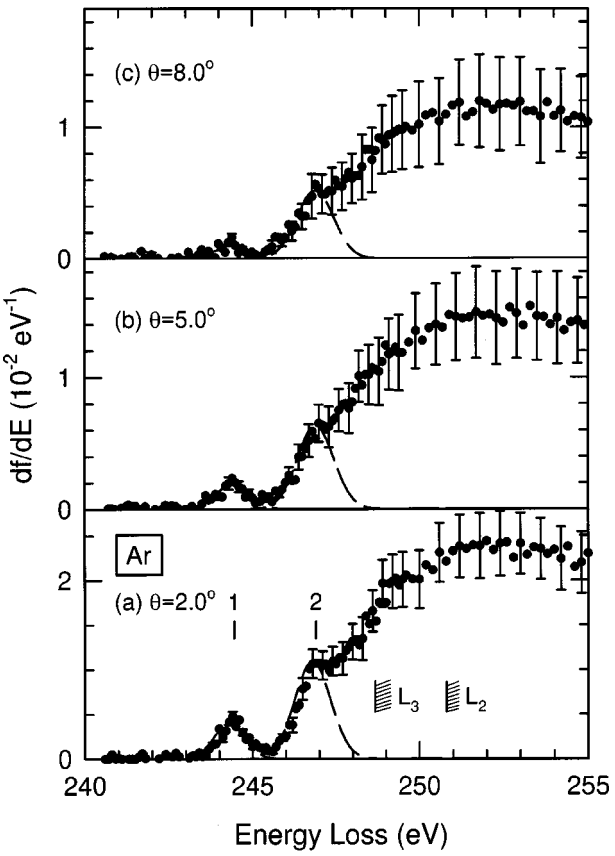

FIG. 6. Absolute electron-energy-loss spectra near the $L_{2,3}$ edge of Ar measured at (a) 2.0°, (b) 5.0°, and (c) 8.0°. Background intensities arising from the valence shell have been removed. Two Gaussian profiles with the appropriate linewidths are used to estimate the intensities of the structures at 244.4 eV (feature 1) and 246.9 eV (feature 2) in a curve-fitting procedure.

[i.e., $3p^5(4s,4s')$ for feature 1 vs $3p^5(5d,5d')$ for feature 3].

C. Electronic structure of the Ar 2*p* shell

Figure 6 shows representative EELS spectra for the energy-loss region near the $L_{2,3}$ edges of Ar obtained at 2.0°, 5.0°, and 8.0°, after the background from the valence-shell contribution has been appropriately removed. The intensities of these inner-shell structures were automatically normalized on an absolute scale after normalization of the valence-shell region, because the entire EELS spectra (up to 300 eV) were obtained in a self-normalized fashion as discussed above. Evidently, except for a general reduction in the overall intensity, there is no discernible difference in the general shape of the electron-impact excitation structure at the larger scattering angles. Using two Gaussian peaks to fit the structure in the 241–248-eV region, we identify two prominent features. The excited states in the inner-shell region have been investigated by photoabsorption [38,39] and small-angle EELS [40,41]. In particular, King *et al.* [40] assigned the peak at 244.4 eV (feature 1) to the promotion of a $2p_{3/2}$ electron to an unoccupied 4*s* Rydberg orbital. The other prominent feature at 246.9 eV (feature 2) can be attributed to an admixture

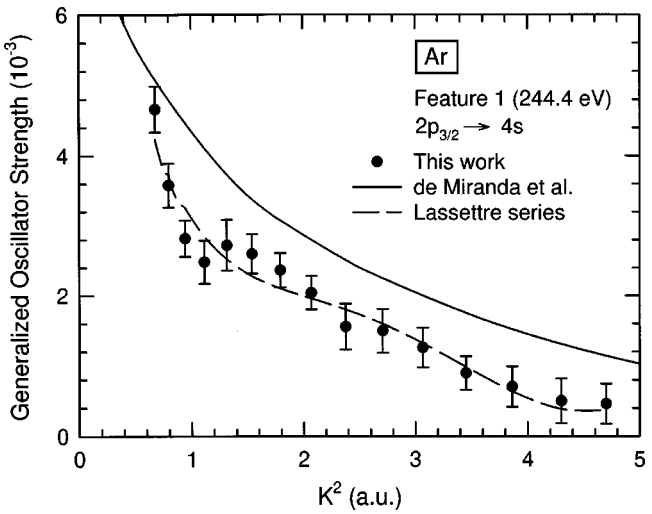

FIG. 7. Absolute generalized oscillator strength as a function of momentum transfer (K) squared for the $2p_{3/2} \rightarrow 4s$ inner-shell transition (at 244.4 eV) in Ar. The present data is compared with the configuration-interaction calculation (solid line) by de Miranda and Bielschowsky [43] that includes relaxation effects. The dashed line corresponds to a semiempirical fit using the Lassettre series.

of dipole-allowed $2p_{3/2} \rightarrow (3d,5s)$ (at 246.927 eV) and $2p_{1/2} \rightarrow 4s'$ transitions (at 246.514 eV) [40], which cannot be resolved with our limited energy resolution. Given the low cross section and its close proximity to the dipole-allowed transitions, it would be very difficult for our present low-resolution spectrometer to identify the dipole-forbidden $2p_{3/2} \rightarrow 4p$ transition at 245.959 eV as observed by King *et al.* [40]. The general decrease in the peak intensities with increasing momentum transfer is consistent with the above assignment that the two prominent features correspond to predominantly dipole-allowed electronic transitions. Only the area corresponding to feature 1 is used to evaluate the GOS at different momentum transfer and the resulting GOS profile for the $2p_{3/2} \rightarrow 4s$ transition is shown in Fig. 7. Although the GOS maximum at $K=0$ would indicate contribution from electronic excitations involving predominantly dipole-allowed transitions, the shape of the GOS profile is complex. The generally broader GOS profile for the $2p_{3/2} \rightarrow 4s$ transition is quite typical for inner-shell transitions [42], in marked contrast to the more abrupt variation commonly observed for valence-shell transitions. The shoulder at $K^2=1.4$ a.u. suggests possible contribution from nondipole-like components. We also compare the experimental GOS profile with a configuration-interaction calculation by de Miranda and Bielschowsky, which took relaxation effects into account [43]. Although there is good accord in the overall shape of the dipole-allowed transition, the calculation does not appear to reproduce both the absolute magnitude and the finer details of the experimental GOS profile (such as the aforementioned shoulder). Quantitative understanding of the GOS profile would therefore require even more sophisticated quantum-mechanical calculations that include more extensive corrections for electron correlation and core-level relaxation effects.

V. CONCLUDING REMARKS

In summary, an improved angle-resolved EELS spectrometer has been used to investigate the nature of some of the more prominent electronic excitations in the valence and $2p$ shells of Ar. The experimental Bethe surface presented here gives a comprehensive picture of the valence-shell electronic structure of Ar. In particular, the GOS profile for the $3p^6 \rightarrow 3p^5(4s,4s')$ transitions has been determined and the locations of the extrema in the GOS profile are found to be in good accord with the published experimental and theoretical results. Furthermore, our GOS profile appears to be in considerably better agreement with calculations based on the Glauber-YFC approximation [18] than the earlier measurements [16,18]. This work also presents the first GOS data for the lowest-lying dipole-forbidden $3p^6 \rightarrow 3p^5(4p,4p')$ transitions and the other dipole-allowed $3p^6 \rightarrow 3p^5(5s,5s',3d,3d')$ preionization-edge transitions in the valence shell, as well as the $2p_{3/2} \rightarrow 4s$ inner-shell transition. Unlike the earlier experimental studies [14,17,18], the GOS profiles in the present work were made absolute independently by using the Bethe sum-rule normalization procedure and do not rely on the accuracy of other data. The excellent agreement in the DOS found for the dipole-allowed features (feature 1 and feature 3) in the valence shell validates the general accuracy (10–15 %) for absolute GOS measurement achievable by the present technique of high-energy angle-resolved EELS. The present work demonstrates the potential of GOS profiles for comprehensive investigation of the prominent excited states in the valence and inner shells, including both the dipole-allowed and the optically inaccessible nondipole states. The GOS profiles of the respective transitions exhibit distinctive features specific to the connecting states. Further experimental investigations of these atomic transitions with an improved energy resolution will provide new benchmarks for the development of more quantitative *ab initio* methods and advanced understanding of the nature of dipole and nondipole excitations in atoms.

ACKNOWLEDGMENT

This work was supported by the Natural Sciences and Engineering Research Council of Canada.

[1] H. Bethe, Ann. Phys. (Leipzig) **5**, 325 1930; H. Bethe, Z. Phys. **76**, 293 (1932).
[2] R. A. Bonham, in *Electron Spectroscopy: Theory, Techniques and Applications*, edited by C. R. Brundle and A. D. Baker (Academic, New York, 1979), Vol. 3, p. 127.
[3] M. Inokuti, Rev. Mod. Phys. **43**, 297 (1971).
[4] E. N. Lassettre and A. Skerbele, in *Methods of Experimental Physics*, edited by D. Williams (Academic, New York, 1974), Vol. 3 (Part B), Chap. 7.2, p. 868.
[5] A. Hamnett, W. Stoll, G. Branton, C. E. Brion, and M. J. van der Wiel, J. Phys. B **9**, 945 (1976).
[6] A. Lahmam-bennani, M. Cherid, and A. Duguet, J. Phys. B **20**, 2531 (1987).
[7] R. Camilloni, E. Fainelli, G. Petracelli, and G. Stefani, J. Phys. B **20**, 1839 (1987).
[8] J. T. Francis, C. C. Turci, T. Tyliszczak, G. G. B. de Souza, B. Kosugi, and A. P. Hitchcock, Phys. Rev. A **52**, 4665 (1995).
[9] J. F. Ying, T. A. Daniels, C. P. Mathers, H. Zhu, and K. T. Leung, J. Chem. Phys. **99**, 3390 (1993).
[10] V. V. Afrosimov, Yu. S. Gordeev, V. M. Lavrov, and S. G. Shchemelinin, Zh. Eksp. Teor. Fiz. **55**, 1569 (1968) [Sov. Phys. JETP **28**, 821 (1969)].
[11] W. McConkey and F. G. Donaldson, Can. J. Phys. **51**, 914 (1973).
[12] J. E. Mentall and H. D. Morgan, Phys. Rev. A **14**, 954 (1976).
[13] D. J. Chornay, G. C. King, and S. J. Buckman, J. Phys. B **17**, 3173 (1984).
[14] W. F. Chan, G. Cooper, X. Guo, G. R. Burton, and C. E. Brion, Phys. Rev. A **46**, 149 (1992).
[15] A. Chutjian and D. C. Cartwright, Phys. Rev. A **23**, 2178 (1980).
[16] T. C. Wong, J. S. Lee, and R. A. Bonham, Phys. Rev. A **11**, 1963 (1974).
[17] G. P. Li, T. Takayanagi, K. Wakiya, H. Suzuki, T. Ajiro, S. Yagi, S. S. Kano, and H. Takuma, Phys. Rev. A **38**, 1240 (1987).
[18] C. E. Bielschowsky, G. G. B. de Souza, C. A. Lucas, and H. M. Boechat Roberty, Phys. Rev. A **38**, 3405 (1988).
[19] R. A. Bonham, J. Chem. Phys. **36**, 3260 (1962).
[20] I. Shimamura, J. Phys. Soc. Jpn. **30**, 824 (1971).
[21] P. S. Ganas and A. E. S. Green, Phys. Rev. A **4**, 183 (1971).
[22] See, for example, J. F. Ying and K. T. Leung, J. Chem. Phys. **101**, 8333 (1994); J. F. Ying and K. T. Leung, Phys. Rev. A **53**, 1476 (1996).
[23] K. T. Leung, J. Electron Spectrosc. Relat. Phenom. **100**, 237 (1999).
[24] X. W. Fan and K. T. Leung (unpublished).
[25] X. W. Fan and K. T. Leung (unpublished).
[26] E. N. Lassettre, J. Chem. Phys. **43**, 4479 (1965); M. A. Dillon and E. N. Lassettre, *ibid.* **62**, 2373 (1975). See also M. A. Dillon, M. Inokuti, and Z. W. Wang, Radiat. Res. **102**, 151 (1985).
[27] M. Inokuti, J. L. Dehmer, T. Baer, and J. D. Hanson, Phys. Rev. A **23**, 95 (1981), and references therein.
[28] J. A. Wheeler and J. A. Bearden, Phys. Rev. **46**, 755 (1934).
[29] Y. K. Kim and M. Inokuti, Phys. Rev. **175**, 176 (1968).
[30] J. W. Cooper, Phys. Rev. **128**, 681 (1962).
[31] C. M. Lee and K. T. Lu, Phys. Rev. A **8**, 1241 (1973).
[32] C. M. Lee, Phys. Rev. A **10**, 584 (1974).
[33] W. B. Westerveld, Th. F. A. Mulder, and J. Van Eck, J. Quant. Spectrosc. Radiat. Transf. **21**, 533 (1979).
[34] S. Tsurubuchi, K. Watanabe, and T. Arikawa, J. Phys. Soc. Jpn. **59**, 497 (1990).
[35] G. M. Lawrence, Phys. Rev. **175**, 40 (1968).
[36] W. M. Huo, J. Chem. Phys. **71**, 1593 (1979).
[37] J. F. Ying, C. P. Mathers, and K. T. Leung, Phys. Rev. A **47**, R5 (1993).
[38] M. Nakamura, M. Sasanuma, S. Sato, M. Watanabe, H. Ya-

mashita, Y. Iguchi, A. Ejiri, S. Nakai, S. Yamaguchi, T. Sagawa, Y. Nakai, and T. Oshio, Phys. Rev. Lett. **21**, 1303 (1968).
[39] R. D. Deslattes, Phys. Rev. **186**, 1 (1969).
[40] G. C. King, M. Tronc, F. H. Read, and R. C. Bradford, J. Phys. B **10**, 2479 (1977).
[41] D. A. Shaw, G. C. King, F. H. Read, and D. Cvejanovic, J. Phys. B **15**, 1785 (1982).
[42] J. F. Ying and K. T. Leung, J. Chem. Phys. **101**, 7311 (1994), and references therein.
[43] M. P. de Miranda and C. E. Bielschowsky, J. Mol. Struct. **282**, 71 (1993).